Sustainable Energy & Fuels

ROYAL SOCIETY OF CHEMISTRY

PAPER

View Article Online
View Journal | View Issue

Cite this: *Sustainable Energy Fuels*, 2026, **10**, 1313

Fewer photons, more hydrogen: effects of dynamic irradiation on light-driven hydrogen evolution by thiomolybdate catalysts

S. Henriette Kolbinger,[a] Laura Haxha,[a] P. Charlotte Schröder,[a] Daniel Kowalczyk,[b] Luis Senz,[a] Luca Schleicher,[a] Arijit Mukherjee,[c] Daniel Malcolm,[a] Corinna L. Kufner,[d] Dirk Ziegenbalg *[b] and Carsten Streb *[a]

Molecular molybdenum sulfide clusters such as $[Mo_3S_{13}]^{2-}$ (**{Mo$_3$}**) are promising earth-abundant catalysts for the light-driven hydrogen evolution reaction (HER). Their catalytic performance strongly depends on the irradiation conditions, which can influence both activity and stability. In this study, the prototype thiomolybdate **{Mo$_3$}** was combined with $[Ru(bpy)_3]^{2+}$ as a photosensitizer (**PS**) to evaluate HER performance under dynamic irradiation conditions, a combination that has not been systematically explored before. A statistical Design of Experiments (DoE) approach was applied to assess the impact of three key parameters, *i.e.*, irradiation intensity, on/off frequency, and duty cycle on the catalytic performance (assessed based on the turnover number). The results identify irradiation intensity as the main control parameter for catalytic activity, followed by duty cycle and on/off frequency. Interactions between frequency and duty cycle underline the importance of dark periods in the irradiation sequence. Optimization of the three key parameters resulted in a 102% increase in hydrogen production compared to continuous irradiation while reducing the required energy input by 25%. Mechanistic studies provide initial insights into photosensitizer and catalyst deactivation under the given irradiation conditions. These findings highlight the potential of controlled pulsed irradiation to improve energy use in light-driven homogeneous HER.

Received 11th November 2025
Accepted 30th January 2026

DOI: 10.1039/d5se01490e

rsc.li/sustainable-energy

Motivation & introduction

Molybdenum sulfides have attracted considerable attention as earth-abundant, noble-metal-free catalysts for the HER.[1–4] Specifically, molecular molybdenum sulfide clusters, so-called thiomolybdates, have been used as molecular prototypes to study reactivity and understand the underlying mechanisms which govern HER activity and catalyst stability.[5–8] Specifically, the prototype thiomolybdate $[Mo_3S_{13}]^{2-}$ (=**{Mo$_3$}**, Fig. 1) has been explored in homogeneous light-driven HER,[5,9] and the system has demonstrated remarkable turnover numbers (TONs) in the tens of thousands.[5] However, **{Mo$_3$}** is highly sensitive to the reaction conditions and shows highly dynamic behavior under catalytic operation.[5,8] In addition, mechanistic studies of **{Mo$_3$}** require precise preparation and careful experimental timing, as the cluster undergoes extensive disulfide ligand exchange reactions over time in solution, which results in time-dependent changes in HER activity, making mechanistic studies challenging.[5,8,10]

Specifically, to-date, there is no information on the effects of irradiation on the HER performance of **{Mo$_3$}** (and on homogeneous HER catalysts in general). Thus, there is a distinct knowledge gap regarding the interplay between irradiation conditions, HER performance and catalyst/photosensitizer

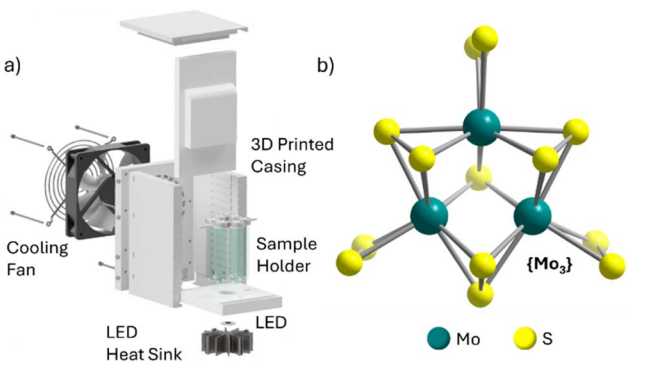

Fig. 1 (a) 3D Scheme of the modular photoreactor corpus[18] and (b) illustration of the $[Mo_3S_{13}]^{2-}$ catalyst.

[a]*Department of Chemistry, Johannes Gutenberg-University Mainz, Duesbergweg 10-14, 55128 Mainz, Germany. E-mail: carsten.streb@uni-mainz.de*

[b]*Institute of Chemical Engineering, Ulm University, Albert-Einstein-Allee 11, 89081 Ulm, Germany. E-mail: dirk.ziegenbalg@uni-ulm.de*

[c]*Institute of Physical Chemistry, Friedrich Schiller University Jena, Helmholtzweg 4, D-07743 Jena, Germany*

[d]*Leibniz Institute of Photonic Technology, Albert Einstein Str. 9, 07745 Jena, Germany*

stability.[11,12] This is despite the fact that it was recently demonstrated that dynamic irradiation of light-driven molecular catalysts can be used to control and improve catalyst stability and consequently, catalytic performance.[13] However, exploration of the complex interplay between all reaction parameters involved is far from trivial and has not been tackled in thiomolybdate catalysis or general HER catalysis to-date.

These aspects are particularly relevant for technological implementation where precise control of light exposure is essential to maximize both photocatalytic efficiency and energy utilization.[14–16] Photochemical processes, in particular, benefit from recent advances in LED technology, which allow for fine-tuned modulation of irradiation intensity, frequency, and pulsing.[17–19] Such dynamic irradiation conditions can offer new insights into the kinetics of light-driven systems and may lead to improved reaction control by identifying and selectively addressing rate-determining steps.[13]

Here, we report the influence of dynamically modulated irradiation on the light-driven HER of **{Mo$_3$S$_{13}$}** when coupled with $[Ru(bpy)_3]^{2+}$ as **PS**. The study assesses the impact of irradiation parameters (irradiation intensity, on/off frequency, and duty cycle) on the catalytic system and uses these data to identify optimized reaction conditions and reveal key correlations between these reaction parameters.[20] A statistical DoE approach is used for these investigations since it enables the reduction of the number of experiments necessary to get all the information to a minimum and identify significant influences and correlations between parameters based on statistical analysis. In addition, combined experimental and theoretical mechanistic studies provide initial insights into the molecular processes which govern the reactivity and stability of this system.

Results and discussion

To understand the fundamental reactivity of the catalytic system under study, we first identified standard conditions (regarding solvent, reagent concentrations, acidity, *etc.*) which are used to comparatively assess the impact of dynamic irradiation.[21,22] This was particularly important as **{Mo$_3$S$_{13}$}** reactivity is known to be dependent on the reaction parameters.[10,23] Thus, the standard system used in all measurements is based on the thiomolybdate catalyst $(NH_4)_2[Mo_3S_{13}]$ (=$(NH_4)_2${**Mo$_3$S$_{13}$**}; c = 0.3 μM), $[Ru(bpy)_3](PF_6)_2$ as a photosensitizer (c = 20 μM) and a buffer solution of ascorbic acid/sodium ascorbate (pH = 4) as a sacrificial electron donor (SED; c = 10 mM) in a methanol : water mixture (9 : 1, v : v). The reaction mixture was irradiated with a monochromatic LED at λ_{max} = 465 nm.[23] Irradiation was performed in a custom-built 3D-printed modular photoreactor with 6 positions, which enables standardized, reproducible irradiation, thus limiting the impact of experimental error.[18] In addition, the system can be used to introduce dynamic irradiation while maintaining all other reactor parameters (irradiation geometry, *etc.*). Note that the reaction mixtures were not stirred as this led to reduced photocatalytic performance in this reactor type as reported previously.[18]

Static irradiation with an LED driver current of 700 mA was chosen as a standard irradiation setting, as this corresponds to an average photon fluence rate rate of 51 nmol s^{-1} cm^{-2}. To ensure comparability, the light power was determined for each of the six individual sample positions of the photoreactor (Fig. 1, for details see the SI). Note that in the following, only the respective LED driver current will be given instead of the light power for clarity and brevity.

Hydrogen evolution was measured after 5 h of static irradiation by gas chromatography for three different sample positions, and the corresponding TON was determined. Different sample positions were used to eliminate systematic errors due to minor differences between the irradiation conditions due to different relative positioning of the sample vial and LED.[18] The measurement was performed six times in total and the standard deviations (SDs) for the measurements were determined. Note that these SDs are due to possible minor leakage of H_2 through the septa and general experimental errors, *e.g.* during preparation of the catalytic samples or slight differences in irradiation intensities in the different positions. These measurements represent the standard benchmark for this work and correspond to an irradiation intensity of 700 mA, a frequency of 0 Hz and a duty cycle of 100% (Fig. 2). Under these irradiation settings a TON of 670 ± 140 was determined.

DoE for dynamic irradiation

With the catalytic benchmark under static conditions established, further analysis of dynamic irradiation was carried out. The influence of dynamic irradiation was studied based on the three main parameters: photon fluence rate (determined from the LED current, 350 mA, 500 mA or 700 mA), LED on/off frequency (2 Hz or 50 Hz, number of full on/off cycles per second) and duty cycle (25% or 75%, on/off time ratio of the LED per cycle). A schematic diagram of the different parameter combinations of duty cycle and irradiation frequency is shown in Fig. 2.

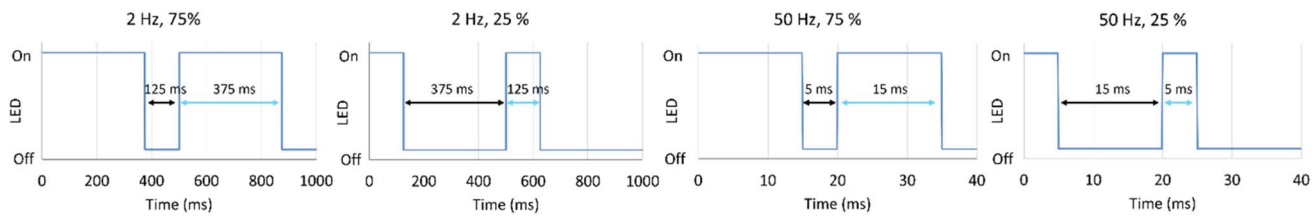

Fig. 2 Detailed illustration of the on/off frequencies and duty cycle used for the experimental studies.

The simultaneous investigation of multiple parameters is challenging, as it can require a large number of experiments, particularly for identifying correlations between individual parameters. Traditionally, the one-factor-at-a-time (OFAT) model is applied to study such influences.[21,22] However, the OFAT model provides no insights into possible interactions between the individual parameters, which can lead to misinterpretation of results.[24] An alternative to address these drawbacks is the use of Design of Experiments (DoE), which we use in the present study. DoE uses a statistical approach to experiment planning and can provide insight into the impact of each parameter and possible interactions between individual parameters. Moreover, it decreases the number of experiments required to get a full overview of the interaction and correlation between individual parameters while enabling the changing of all parameters simultaneously.[20] For this work a full factorial screening design was selected to obtain a complete overview of individual influences of the parameters and their possible interactions. An experiment plan was generated using Minitab Statistical Software 22. The order of experiments was randomized. The detailed experimental plan is provided in the SI.

Each experiment was carried out in triplicate using the standard experimental conditions described above ($(NH_4)_2${**Mo$_3$**}; c = 0.3 μM, $[Ru(bpy)_3](PF_6)_2$; c = 20 μM, buffer solution of ascorbic acid/sodium ascorbate (pH = 4) as the SED; c = 10 mM in a methanol : water mixture 9 : 1, v : v, no stirring) as well as the respective parameter settings as outlined above. An overview of the resulting H_2 TONs is shown in Fig. 3 and SI, Table S4. Based on these data, and using TONs as the performance parameter, we obtained the main effect diagrams shown in Fig. 3.

The main effect diagram can be interpreted as follows: the individual graphs show the influence of the lower *vs.* the higher value setting. The vertical range covered by a graph in terms of the responding parameter indicates the extent of the influence of the respective parameters. With that in mind, the main effect diagram can be interpreted. An increased frequency has a negative impact on the TON while an increased LED current and duty cycle have a positive impact. Furthermore, the LED current causes the biggest changes in the TON. This implies that the LED current and therefore light intensity have the biggest influence on the HER performance of the system, followed by the duty cycle and the on/off frequency. These results suggest that at high light power and high duty cycle, more photons are provided to the reaction, resulting in higher catalytic turnover. By contrast, the negative trend observed for frequency is less intuitive, as changing frequency does not alter the total energy input. Further analysis is therefore needed to rationalize this observation.

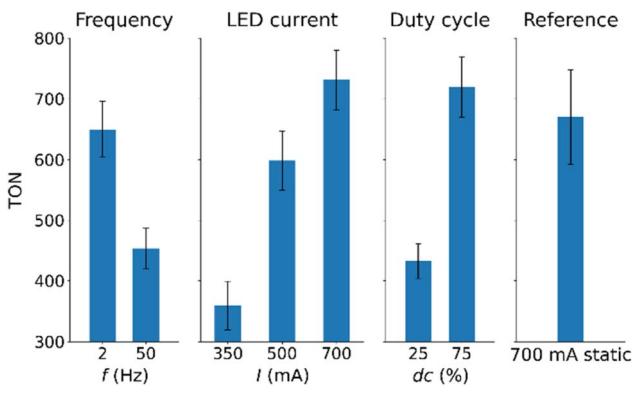

Fig. 3 Main effect diagram for the individual parameters: on/off frequency, LED current and duty cycle. Plot of the average TON *vs.* frequency, LED current and duty cycle. The TON of the reference experiment (static conditions: 700 mA, 0 Hz, 100%) is shown for comparison. Error bars represent the standard error of the mean.

One possible explanation for this observation is that exchange of the terminal disulfide ligands at {**Mo$_3$**} is photon fluence rate dependent, so that high photon fluence rates can result in increased deactivation. This hypothesis will be tested later in this work. Based on earlier work,[5] we propose that the catalyst degradation might follow a similar mechanism as discussed for the photosensitizer $[Ru(bpy)_3]^{2+}$,[25] In both cases, loss of terminal chelating ligands ({**Mo$_3$**}: S_2^{2-}; photosensitizer: bpy) requires cleavage of two coordinative bonds to result in deactivation. At low photon fluence rates this is less likely compared with high photon fluence rates, offering a plausible explanation for the photon fluence rate-dependency of deactivation. Note that the loss of these terminal ligands is expected to have a major impact on catalytic reactivity as these sites are discussed as the reactive centers for HER by {**Mo$_3$**}.[8]

In the next step, we analyzed possible interactions between the parameters which are not captured by the main effect diagram. This is visualized in interaction diagrams, see Fig. 4.

In general, interaction diagrams indicate the presence of interactions between two parameters when the connecting lines between individual experimental series are non-parallel or even cross (Fig. 4, center). In contrast, no interactions are present when the connecting lines are parallel (*e.g.* Fig. 4, left and right). Here, we observe interactions between the on/off frequency and the duty cycle as shown in Fig. 4, center. Since the on/off frequency and duty cycle together describe the duration of the irradiation and dark phases, our findings indicate that certain dark-phase lengths are favorable for reaching higher TONs. This insight will be used later to identify optimized irradiation conditions for this reaction.

Before aiming at optimized reaction conditions, it is important to assess whether most of the changes in reactivity observed are due to the parameters tested, or caused by other, untested (or unknown) parameters. This can be assessed based on the R^2 value, which is a goodness-of-fit parameter to assess whether enough parameters have been used in the data analysis, or whether more complex models using additional parameters would be better suited.[26] Here, the analysis of variance (ANOVA) for this data determined R^2 to be 70.6%, indicating that *ca.* 71% of the TON changes observed are due to the parameters studied, while *ca.* 29% of the TON changes observed are due to other, unknown factors (*e.g.* minor differences in irradiation geometry, H_2 gas leakage, general experimental errors, *etc.*). This indicates that most TON changes are explained by the parameters studied, which is a sufficient basis for subsequent TON optimization studies.

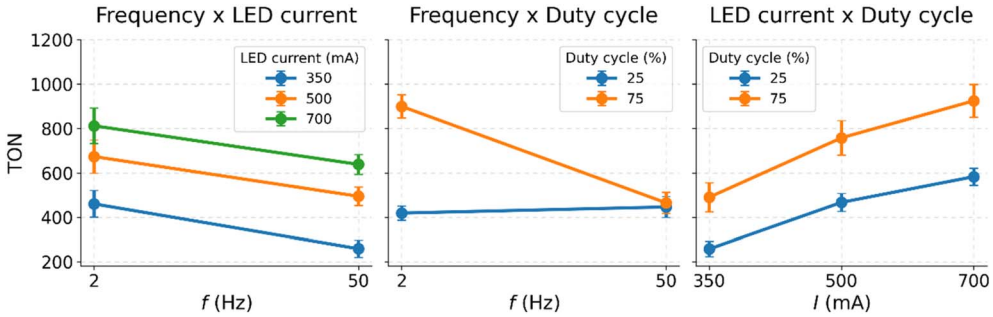

Fig. 4 Interaction diagram to explore interdependence of two parameters. Left: Average TONs *vs.* on/off frequency for different LED currents; center: average TONs *vs.* on/off frequency for different duty cycles; right: average TONs *vs.* LED current for different duty cycle. Error bars represent the standard error of the mean.

Finally, the DoE analysis enables prediction of the optimal parameter settings (within the investigated parameter space) for maximizing TON. Based on the factorial model, the predicted optimum is an on/off frequency of 2 Hz, an LED current of 700 mA, and a duty cycle of 75%. To validate this prediction, HER experiments were performed under these conditions. As summarized in Table 1, the resulting TON increased substantially compared to the best conditions shown in Fig. 4 as well as compared to the standard setting described above. Notably, the optimum uses a 75% duty cycle and reaches a TON of 1350, whereas a static experiment under otherwise comparable conditions yields only TON = 670. Thus, the optimum setting results in a 102% higher TON while requiring 25% less energy input. Also, TON normalized to energy input increases by a factor of approximately three (Table 1). This unexpected result indicates that introducing dark phases can significantly enhance catalytic turnover while simultaneously reducing energy consumption. Possible explanations include light-induced degradation of reaction components under continuous irradiation, or a positive role of dark phases in specific catalytic steps; these hypotheses are discussed further below.

To gain quantitative insights into the energy costs to produce hydrogen in our system, we set out to determine the photonic efficiency (PE) under different irradiation conditions. The photonic efficiency (PE = $n(H_2)/n$(incident photons))[27] was calculated for each parameter setting to identify the most photon-efficient setting. The calculated PEs for all irradiation settings can be found in the SI. The parameter setting with the highest PE was found to be 500 mA, 50 Hz and 25%.

First, for static irradiation (Table 2, entries 1 and 2), we observed identical PEs at different photon fluence rates q_{ph}, indicating that photon fluence rate does not alter the underlying hydrogen evolution mechanisms under continuous, static irradiation. This behavior is also observed in the main effect diagram (Fig. 3), where a linear increase of LED current results in a linear increase of TON, indicating that the mechanism of hydrogen evolution under static irradiation remains unchanged over the photon fluence rate range studied. However, under pulsed irradiation conditions (Table 2, entries 3 and 4) we observe that decreasing photon fluence rate results in increasing photonic efficiencies. Most notably, under optimized dynamic conditions (500 mA, 50 Hz, 25%, Table 2, entry 4), the PE increased by a factor of four compared to the static benchmark (Table 2, entry 2). This highlights that dynamic irradiation affects the hydrogen evolution process, most likely by impacting reactions which occur on the same timescale as the dynamic changes (*i.e.*, millisecond timescale). This interpretation suggests that slower processes (*e.g.*, diffusion, aggregation, and ion pairing) are impacted, rather than the faster photophysical/photochemical processes (excitation and charge-separation). Future work will explore potential reaction paths impacted by dynamic irradiation using combined *in situ* experimental studies and theoretical computations.

Table 1 Average TON for standard and optimized irradiation settings

Irradiation setting	700 mA static	700 mA, 2 Hz, 75%
TON	670 ± 140	1350 ± 160
Energy input	65 mWh	48.75 mWh
TON/energy input	10.3 mWh^{-1}	27.7 mWh^{-1}

The results found for TON and PE as a function of the different irradiation settings are also visualized in a 3D plot in Fig. 5. The 3D plot for the TON shows that the surfaces for the different LED currents do not cross each other but seem to be parallel. The LED current shifts the TON only up and down while frequency and duty cycle have different influences. For the PE, the surfaces of the different LED currents intersect. The influence of all 3 key parameters on PE seems to be more complex. The 3D representations clearly show that for achieving the two different optimization objectives, *i.e.* TON or PE, different irradiation conditions must be set.

To better understand the trends observed, it is critical to assess the stability of the **PS** and **{Mo_3}** under the given reaction conditions. Note that irradiation of the **PS** can lead to degradation (photobleaching), which will impact the observed catalytic reactivity.[12]

Decay rate constants of $[Ru(bpy)_3]^{2+}$

As noted above, the photobleaching of the **PS** can be a limiting factor for the catalytic performance of the system. To evaluate whether dynamic irradiation can lead to decreased

Table 2 Calculated photonic efficiencies PE, and average photon fluence rate q_{Ph} for standard, TON-optimized irradiation settings and the irradiation setting with the highest PE found

Entry no.	Setting	PE (10^{-3})	q_{Ph} (nmol s^{-1} cm^{-2})	TON (–) after 5 h of irradiation
1	350 mA static	0.7 ± 0.4	27 ± 4	340 ± 120
2	700 mA static	0.7 ± 0.2	51 ± 4	670 ± 140
3	700 mA, 2 Hz, 75%	1.9 ± 0.3	38 ± 3	1350 ± 160
4	500 mA, 50 Hz, 25%	3.0 ± 1.1	9 ± 1	520 ± 140

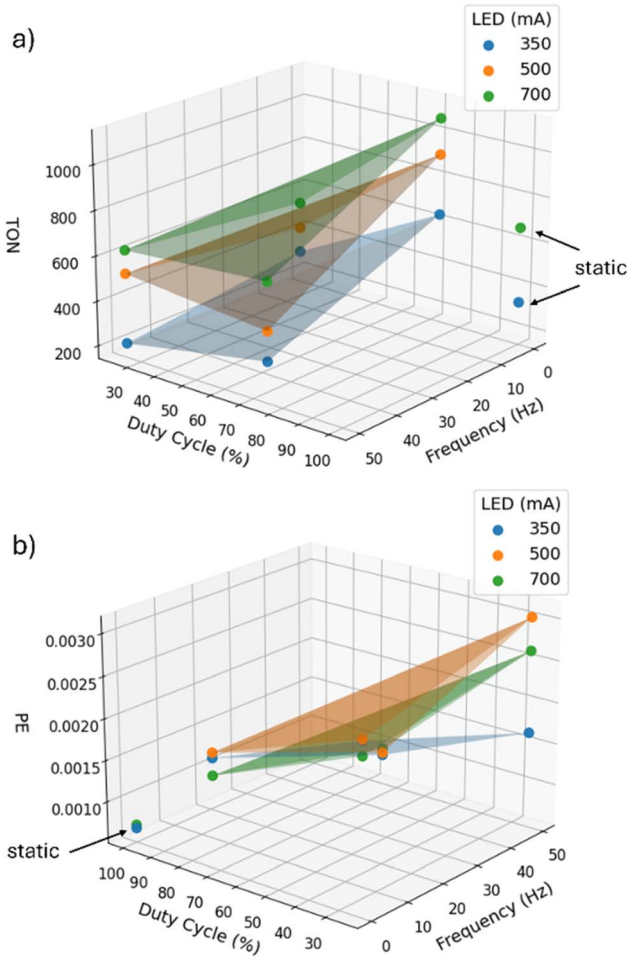

Fig. 5 (a) 3D-plot of TON *vs.* duty cycle and frequency for different LED currents. (b) 3D-plot of PE *vs.* duty cycle and frequency for different LED currents. Single points represent the static benchmark experiments.

photobleaching, the decay rate constants of the **PS** were determined under different irradiation conditions using UV-Vis spectroscopy. To this end, the decrease of the characteristic MLCT transition at 452 nm was monitored over 5 h of irradiation ($\lambda_{irradiation}$ = 465 nm). The degradation of the **PS** was investigated in two different systems: (1) **PS** in methanol (Ru) and (2) the catalytic system as used in the experiments above (RuSEDCat). The concentration of **PS** was kept identical throughout the experimental series. Decay quantum yields Φ of the degradation of the **PS** were calculated for the two systems irradiated under different irradiation settings.[28] The data are shown in Table 3.

The decay quantum yields for **PS** in pure methanol solutions show a clear trend, in that increasing photonic energy input results in more photobleaching and higher decay quantum yields. We note a particularly low decay quantum yield (*i.e.*, high **PS** stability) for the 500 mA, 50 Hz, 25% setting. Essentially, the data show a linear relationship between photon fluence rate and decay quantum efficiency (Fig. 6). This is plausible, as higher photonic excitation rates can lead to an increased population of antibonding orbitals on the PS, resulting in increased loss of the bpy ligand, which is a known deactivation mechanism for the **PS**.[25,29–31] Thus, lower photon fluence rate will result in reduced ligand loss, as bpy is a chelating ligand which requires the cleavage of two Ru–N bonds for complete bpy removal.[32] To further study this observation, future studies will focus on detailed time-resolved photophysical studies and complementary theoretical calculations.

In the catalytic system RuSEDCat, we observe a different trend: in general, the decay quantum yields are higher than those for the pure Ru system (except for the high-fluence rate situation, *i.e.*, 700 mA static, Table 3 and Fig. 6). This indicates that other components now present in the system (*e.g.* SED, catalyst, *etc.*) increase **PS** degradation. Notably, here, increased photon fluence rate results in decreased decay quantum efficiency (Fig. 6), which is the opposite trend to what we observed for the **PS** alone. These initial data suggest that operating the full catalytic system (RuSEDCat) at higher photon fluence rate is beneficial to **PS** stability. One underlying molecular feature which can impact irradiation stability of the PS is the formation of **PS**-SED adducts, which we observed (based on their characteristic UV-Vis absorbance at 532 nm, see SI, Fig. S4–S11).[33] Importantly, when linking PS stability and optimized reaction conditions, we note no major difference in the decay quantum efficiencies for the **PS** between the TON-optimized irradiation conditions (700 mA, 2 Hz, 75%) compared to standard conditions (700 mA, static). This suggests that decreased photobleaching (and thus, higher **PS** stability) is not the major driver for the higher TONs observed under dynamic irradiation, and in fact, the given dynamic conditions can result in slightly increased PS degradation. For this reason, we subsequently examined the photostability of the catalyst.

Photodegradation of {Mo_3}

{Mo_3} is a red compound and shows visible light-absorption. In a methanol : water mixture (9 : 1, v : v), characteristic absorption

Table 3 Decay quantum yields Φ and time-averaged photon fluence rates q_{Ph} for the two systems Ru ($c([Ru(bpy)_3]^{2+}) = 20$ μM in MeOH) and RuSEDCat ($c(\{Mo_3\}) = 0.3$ μM, $c([Ru(bpy)_3]^{2+}) = 20$ μM, $c(SED) = 10$ mM in MeOH : H_2O, 9 : 1, v : v) under different irradiation settings

Irradiation setting	q_{Ph} (nmol s^{-1} cm^{-2})	Φ_{Ru} (10^{-5})	$\Phi_{RuSEDCat}$ (10^{-5})
700 mA static	51 ± 4	4.16 ± 0.01	3.2 ± 0.2
500 mA static	37 ± 4	3.330 ± 0.001	4.8 ± 0.5
700 mA, 2 Hz, 75%	38 ± 3	3.7 ± 0.1	4.1 ± 0.1
500 mA, 50 Hz, 25%	9 ± 1	1.2 ± 0.2	8 ± 1

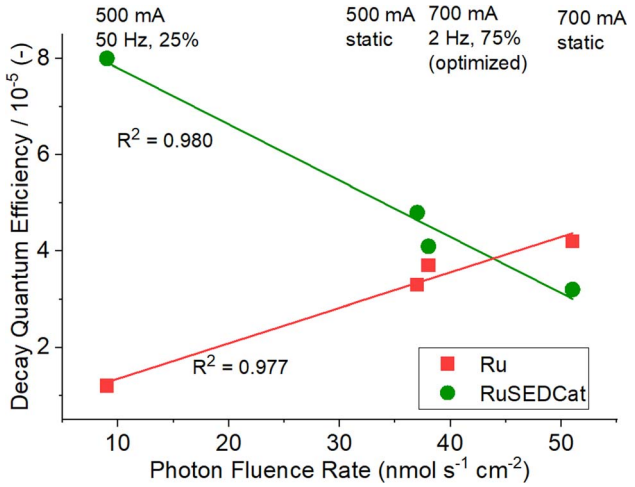

Fig. 6 Decay quantum efficiencies Φ_{Ru} and $\Phi_{RuSEDCat}$ depending on photon fluence rate q_{Ph}. The data show linear dependencies and different trends depending on the reaction and irradiation conditions.

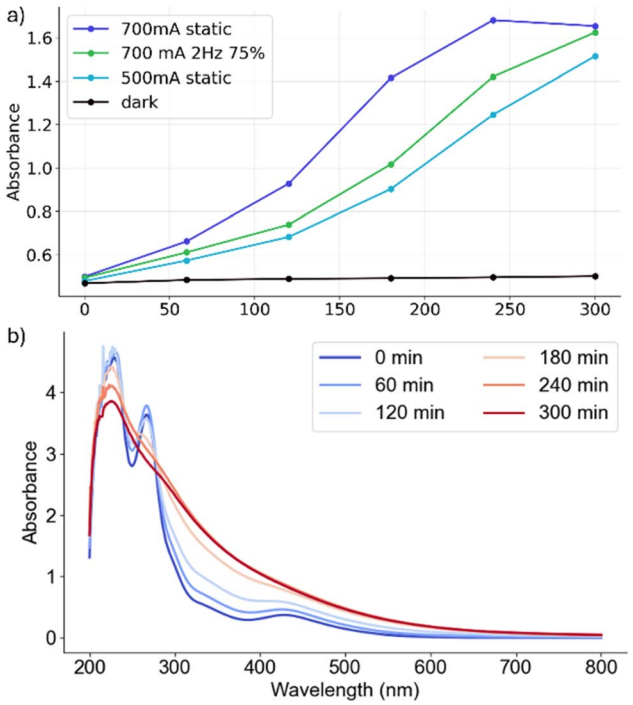

Fig. 7 (a) Absorbance at 340 nm over the course of 5 h for the four $\{Mo_3\}$ solutions. One was irradiated statically at 700 mA, one was irradiated dynamically (700 mA, 2 Hz, 75%), and the third one was irradiated statically at lower intensity (500 mA). The fourth solution was not irradiated. (b) Time-dependent UV-Vis spectra of $\{Mo_3\}$ ($c = 0.1$ mM) in MeOH : H_2O (9 : 1, v : v) under static irradiation (700 mA, 465 nm).

bands are observed at $\lambda_{max} = 428$ nm, 268 nm and 233 nm (spectra are shown in SI, Fig. S12 and S13). The absorption band at 428 nm is likely attributed to a disulfide-to-molybdenum LMCT transition, as supported by DFT calculations (see the SI).

To examine the photostability of $\{Mo_3\}$, we performed time dependent UV-Vis spectroscopy over 5 hours using the same solvent conditions as used in the catalytic studies (methanol : water mixture (9 : 1, v : v)). Three conditions were examined: static irradiation, dynamic irradiation (both using LED-irradiation at 465 nm), and in the absence of light. Under irradiation, the absorption bands at 428 nm and 268 nm gradually merge into a broad shoulder, and the spectra show fewer distinct peaks (Fig. 7). A broad absorption feature between 300 and 350 nm emerges, which increases during irradiation. Based on preliminary TD-DFT-calculations (see the SI), we assign this new band to a previously reported, ligand-exchanged derivative, $[Mo_3S_{13-x}(H_2O)_x]^{(2-x)-}$ ($x = 2$, 4, 6).[5,8] Based on previous literature, it is likely that under the given conditions, the reaction system contains a mixture of species with varying degrees of ligand substitution (x).[5] Note that DFT calculations of the ligand-exchanged $\{Mo_3\}$ species support these findings and indicate that with increasing degree of ligand substitution, the characteristic spectral features disappear, and lead to a broad absorption in the region of 200–350 nm (for details see the SI). In contrast to the spectral changes observed under irradiation, the non-irradiated solution (Fig. 7) shows no significant changes in absorption, confirming that the observed structural transformation of $\{Mo_3\}$ is light-induced.

Next, we examined the rate of absorption change at comparable photon fluence rate (*i.e.*, 700 mA, 2 Hz, 75%, $q_{Ph} = 37$ nmol s^{-1} cm^{-2}, and 500 mA static, $q_{Ph} = 38$ nmol s^{-1} cm^{-2}). Here, we observe that the change in absorption is in a comparable range (within the error margins), suggesting that catalyst deactivation is linked to photon fluence rate, and is not significantly affected by the dynamic irradiation conditions. This is in line with our hypothesis that irradiation induces structural changes in $\{Mo_3\}$ which eventually result in formation of the inactive $[Mo_3S_7(H_2O)_6]^{4+}$. These changes are mainly driven by photonic excitation and therefore the deactivation rate increases with increasing photon fluence rate. Detailed analysis of the data also shows that the absorbance of this band

reaches a maximum after ~4 h under 700 mA static irradiation conditions and subsequently decreases, which may indicate two competitive processes, such as formation of the observed species and subsequent photobleaching at high irradiation intensities.

In sum, these data show that PS and catalyst degradation are controlled by photon fluence rate and increase with increasing photon fluence rate (*i.e.*, energy input); however, they are not directly linked to the dynamic irradiation conditions. Thus, further experimental studies using time-resolved spectroscopy, as well as theoretical calculations and computational modelling of mass transport within the system are required to establish the principal mechanisms of dynamic irradiation.

Conclusions

In sum, we report first insights into the influence of dynamic irradiation on the HER activity of thiomolybdate clusters. Systematic analyses based on Design of Experiments show that the irradiation intensity has the biggest effect on the catalytic activity (based on TON assessment), followed by duty cycle and on/off frequency. Under TON-optimized conditions, we were able to increase the TON by +102% using 25% less energy compared with the static reference conditions. Also, optimization of the photonic efficiency was possible, leading to an approximately threefold increase in TON normalized to the energy input. Initial mechanistic studies shed light on the dependency of photosensitizer and catalyst deactivation on photon fluence rate, and reveal that total photon fluence rate, rather than dynamic conditions controls the system stability. In future, these insights can be used to determine how dynamic irradiation can be used to enable more efficient hydrogen evolution conditions, resulting in more energy- and resource-efficient photocatalysis.

Conflicts of interest

There are no conflicts to declare.

Data availability

Data for this article, including experimental, analytical, catalytic and computational data are available at https://zenodo.org at https://doi.org/10.5281/zenodo.17493789.

Supplementary information (SI): experimental, catalytic and theoretical details. See DOI: https://doi.org/10.1039/d5se01490e.

Acknowledgements

This research was funded by the Deutsche Forschungsgemeinschaft DFG as part of the collaborative research center TRR234 “CataLight” (364549901), projects A05 and C06. Further financial support by Johannes Gutenberg-University Mainz, the HaVo-Stiftung and the Top-Level Research Area “SusInnoScience” is gratefully acknowledged. Furthermore, we would like to acknowledge financial support from the Leibniz-Association (Leibniz-Junior Research group, K197/2024) and the Carl Zeiss Foundation (Nexus-Program, P2023-09-027). Moritz Jahn is gratefully acknowledged for synthesizing the catalyst.

References

1 C. G. Morales-Guio and X. Hu, *Acc. Chem. Res.*, 2014, **47**, 2671–2681.
2 D. Merki and X. Hu, *Energy Environ. Sci.*, 2011, **4**, 3878–3888.
3 T. Wang, H. Xie, M. Chen, A. D'Aloia, J. Cho, G. Wu and Q. Li, *Nano Energy*, 2017, **42**, 69–89.
4 J. D. Benck, T. R. Hellstern, J. Kibsgaard, P. Chakthranont and T. F. Jaramillo, *ACS Catal.*, 2014, **4**, 3957–3971.
5 M. Dave, A. Rajagopal, M. Damm-Ruttensperger, B. Schwarz, F. Nägele, L. Daccache, D. Fantauzzi, T. Jacob and C. Streb, *Sustain. Energy Fuels*, 2018, **2**, 1020–1026.
6 R. A. Sheldon, *Chem. Soc. Rev.*, 2012, **41**, 1437–1451.
7 M. L. Grutza, A. Rajagopal, C. Streb and P. Kurz, *Sustain. Energy Fuels*, 2018, **2**, 1893–1904.
8 S. Batool, M. Langer, S. N. Myakala, M. Heiland, D. Eder, C. Streb and A. Cherevan, *Adv. Mater.*, 2024, **36**, 2305730.
9 Y. Lei, M. Yang, J. Hou, F. Wang, E. Cui, C. Kong and S. Min, *Chem. Commun.*, 2018, **54**, 603–606.
10 B. Seo and S. H. Joo, *Nano Convergence*, 2017, **4**, 1–11.
11 D. Ziegenbalg, A. Pannwitz, S. Rau, B. Dietzek-Ivanšić and C. Streb, *Angew. Chem., Int. Ed.*, 2022, **61**, e202114106.
12 B. Limburg, E. Bouwman and S. Bonnet, *ACS Catal.*, 2016, **6**, 5273–5284, DOI: 10.1021/acscatal.6b00107.
13 M. Sender, F. Huber, M. Moersch, D. Kowalczyk, J. Hniopek, S. Klingler, M. Schmitt, S. Kaufhold, K. Siewerth, J. Popp, B. Mizaikoff, D. Ziegenbalg and S. Rau, *ChemSusChem*, 2022, **15**, 495–513.
14 A. A. Adesina, *Catal. Surv. Asia*, 2004, **8**, 265–273.
15 L. Candish, K. D. Collins, G. C. Cook, J. J. Douglas, A. Gómez-Suárez, A. Jolit and S. Keess, *Chem. Rev.*, 2022, **122**, 2907–2980.
16 S. L. Y. Tang, R. L. Smith and M. Poliakoff, *Green Chem.*, 2005, **7**, 761–762.
17 D. Kowalczyk, G. Knorr, K. Peneva and D. Ziegenbalg, *React. Chem. Eng.*, 2023, **8**, 2967–2983.
18 D. Kowalczyk, P. Li, A. Abbas, J. Eichhorn, P. Buday, M. Heiland, A. Pannwitz, F. H. Schacher, W. Weigand, C. Streb and D. Ziegenbalg, *ChemPhotoChem*, 2022, **6**, e202200044.
19 H. E. Bonfield, T. Knauber, F. Lévesque, E. G. Moschetta, F. Susanne and L. J. Edwards, *Nat. Commun.*, 2020, **11**(1), 1–4.
20 S. A. Weissman and N. G. Anderson, *Org. Process Res. Dev.*, 2015, **19**, 1605–1633.
21 G. E. P. Box, W. G. Hunter and J. S. Hunter, *Statistics for Experimenters*, Wiley, New York, 1978.
22 R. Carlson and J. Carlson, *Design and Optimization in Organic Synthesis*, Google Books, 2nd edn, 2005.
23 M. Heiland, R. De, S. Rau, B. Dietzek-Ivansic and C. Streb, *Chem. Commun.*, 2022, **58**, 4603–4606.
24 V. Czitrom, *Am. Statistician*, 1999, **53**, 126–131.

25 I. M. Dixon, S. Bonnet, F. Alary and J. Cuny, *J. Phys. Chem. Lett.*, 2021, **12**, 7278–7284.
26 Interpretieren der wichtigsten Ergebnisse für Einfache ANOVA - Minitab, https://support.minitab.com/de-de/minitab/help-and-how-to/statistical-modeling/anova/how-to/one-way-anova/interpret-the-results/key-results/#step-4-determine-how-well-the-model-fits-your-data, accessed 1 September 2025.
27 N. Serpone, *J. Photochem. Photobiol., A*, 1997, **104**, 1–12.
28 A. Salinaro, A. V. Emeline, N. Serpone, J. Zhao, H. Hidaka and V. K. Ryabchuk, *Pure Appl. Chem.*, 1999, **71**, 321–335.
29 A. Soupart, F. Alary, J. L. Heully, P. I. P. Elliott and I. M. Dixon, *Inorg. Chem.*, 2020, **59**, 14679–14695.
30 A. Soupart, F. Alary, J.-L. Heully, P. I. P. Elliott and I. M. Dixon, *Coord. Chem. Rev.*, 2020, **408**, 213184.
31 K. Eastham, P. A. Scattergood, D. Chu, R. Z. Boota, A. Soupart, F. Alary, I. M. Dixon, C. R. Rice, S. J. O. Hardman and P. I. P. Elliott, *Inorg. Chem.*, 2022, **61**, 19907–19924.
32 A. P. Demchenko, *Methods Appl. Fluoresc.*, 2020, **8**, 022001.
33 R. S. Khnayzer, V. S. Thoi, M. Nippe, A. E. King, J. W. Jurss, K. A. El Roz, J. R. Long, C. J. Chang and F. N. Castellano, *Energy Environ. Sci.*, 2014, **7**, 1477–1488.